This is a non-peer-reviewed preprint submitted to EarthArXiv.

National-scale mapping locates the mismatch between perceived and assessed flood risk in India

Pratyush Tripathy[1,*], Surabhi Upadhyay[2], Okikiola Michael Alegbeleye[3], Emine Senkardesler[4], Deepika Pingali[5], Emily Goddard[6], Jagadish Thaker[7], Anthony Leiserowitz[6], and Jennifer R. Marlon[6]

[1]*Department of Geography, University of California, Santa Barbara, CA, USA*
[2]*Hydrologic Science and Engineering, Colorado School of Mines, Golden, CO, USA*
[3]*School of the Environment, Washington State University, Pullman, WA, USA*
[4]*School of Information Sciences, University of Illinois Urbana-Champaign, IL, USA*
[5]*Department of Agricultural and Consumer Economics, University of Illinois Urbana-Champaign, IL, USA*
[6]*Yale School of the Environment, Yale University, New Haven, CT, USA*
[7]*School of Communication and Arts, University of Queensland, Brisbane, Australia*
[*]*Corresponding author: ptripathy@ucsb.edu*

September 22, 2026

Abstract

Flood risk management assumes that people in hazardous places recognize the danger they face, but evidence on flood risk perception remains sparse in South Asia, home to much of the world's flood-exposed population. India has more than 600 million people exposed to inland flood hazards and the highest flood-related mortality in Asia, yet no national evidence base on flood risk perception. Here we combine a nationally representative survey of 10,704 Indian adults with a Multilevel Machine Learning with Poststratification (MMLP) approach to estimate flood risk perception for all 633 districts, and compare these against assessed hazard from the flood record. Perceived and assessed risk diverge by more than 30 percentage points in over half of districts, well beyond the uncertainty in our estimates. Districts that most sharply under-perceive risk are concentrated in Assam, Kerala, and Andhra Pradesh, while over-perception is widespread across northern, central, and northeastern states. These mismatches follow state boundaries, with state explaining nearly three times as much of the variance as district-level hydrology, climate, education, vulnerability, and news combined. This makes flood risk perception a measurable input for adaptation planning, and provides a method transferable to any country where hazard is well measured but perception is not.

Keywords: Flood risk; Risk perception; Poststratification; Risk communication; India

1 Introduction

Floods displace communities, destroy livelihoods, and leave lasting economic and social damage across diverse settings (Rentschler et al., 2022). While physical models to predict flood extent and satellite-based tools to map inundation have advanced rapidly (Tripathy & Malladi, 2022), the social dimensions of flood risk remain poorly understood (Bubeck et al., 2012; Kellens et al., 2013). Satellite observations of 913 flood events between 2000 and 2018 show that the share of the world's population exposed to floods grew over this period, as settlement in flood-prone areas outpaced population growth elsewhere (Tellman et al., 2021). This imbalance matters because how people perceive flood risk shapes household preparedness, responses to early warnings, evacuation decisions, and support for adaptation investments (Kellens et al., 2011; Lechowska, 2018; Raaijmakers et al., 2008). India presents the most pressing context in which to address this imbalance, given the size and scale of flood impact in the country. More than 600 million people in India are exposed to inland flood hazards (Moody's Analytics, 2024). India also has the highest flood-related mortality rate in Asia (Kumar et al., 2022; M. P. Mohanty et al., 2020) and a population at risk projected to increase sixfold by 2040 (Jacinth Jennifer et al., 2022). But exposure alone does not determine outcomes; what matters is how communities perceive risk and prepare for it. The state of Odisha in India, for example, reduced cyclone fatalities from the thousands in 1999 to fewer than 100 during Cyclone Fani in 2019 by adopting a community-centered, zero-casualty preparedness model (Ratna et al., 2025).

Strengthening preparedness is difficult to achieve uniformly across India because the flood hazards communities face vary widely. In Bihar, riverine flooding seasonally disrupts agriculture and displaces farming communities, whereas in Assam, the same monsoon systems damage infrastructure and isolate regions for months (Roy et al., 2023; Sahani et al., 2023). Coastal flooding in Andhra Pradesh and Odisha can drive saline water intrusion, contaminating soils and disrupting agricultural livelihoods for years after floodwaters recede (Jain et al., 2025; S. R. Panda et al., 2021). In Himalayan states such as Uttarakhand, flash floods often strike communities with little historical exposure and limited adaptive capacity (Nagamani et al., 2024), a pattern underscored by the August 2026 glacial flood on the Nepal–Tibet border, which echoed the 2021 Chamoli disaster and killed hundreds within hours (The New York Times, 2021, 2026). These patterns are all intensified by climate change through more extreme precipitation and rising seas (Dhiman et al., 2019), which increase both the frequency and severity of floods.

Understanding where and why greater preparedness is needed requires comparing perceived risk, for example, how worried people are about flooding, against assessed risk estimated from physical evidence (Kellens et al., 2011; Lechowska, 2018; Raaijmakers et al., 2008; Rentschler et al., 2022). Where the two align, communities are more likely to prepare, heed warnings, and support adaptation; where they diverge, social responses are often poorly matched to actual conditions (Bubeck et al., 2012). Under-perception in high-risk areas can delay appropriate flood responses and increase losses, while over-perception in low-risk areas may indicate unidentified risks or unnecessary anxiety that erodes institutional trust and diverts resources from more pressing hazards. Identifying where these gaps exist is thus a precondition for effective flood risk management.

These gaps arise because perceived and assessed risks draw on fundamentally different sources (Slovic et al., 2004). Assessed risk rests on the physics of flooding and the record of past events, whereas perception also reflects how well people believe they can cope, which often reflect social and institutional conditions that physical estimates are not designed to capture. For instance, under-perception can arise in several ways: trust in protective infrastructure such as embankments and dams can foster a false sense of security even where structural vulnerability remains high (Grothmann & Reusswig, 2006; Terpstra, 2011); flood experience without severe personal loss can dull perceived risk over time (Bubeck et al., 2012); and residents may discount risk they regard as an institutional responsibility rather than a personal one (Wachinger et al., 2013). On the other hand, over-perception can arise when media coverage amplifies memorable or emotionally charged events beyond what the flood record shows (Kellens et al., 2013). Perception-risk gaps thus reflect the specific experiences, infrastructures, and institutions of particular places.

Capturing such place-specific gaps requires spatially resolved evidence on both hazard and perception. While India's flood hazard has been mapped extensively (Dasgupta et al., 2024; National Remote Sensing Centre (NRSC), 2023; Vegad et al., 2024), evidence on flood risk perception remains fragmented and limited in scale, despite a substantial theoretical and empirical literature (Kellens et al., 2011; Lechowska, 2018; Raaijmakers et al., 2008). India's broader climate risk perception has received some national attention, including surveys of public perceptions of rainfall change and global warming (Howe et al., 2014; Thaker et al., 2020), consistent with international evidence that climate risk perception varies systematically across populations (Lee et al., 2015). Spatially resolved estimates of climate opinion have been produced for the United States using multilevel regression with poststratification, yielding validated county- and district-level estimates of beliefs, risk perceptions, and policy preferences (Howe et al., 2015, 2019). The approach has since been applied to extreme weather hazards, including flooding, across the contiguous United States (Allan et al., 2020), and to climate change concern across Chinese provinces and cities (Xia et al., 2025). National-scale perception mapping has therefore developed largely apart from the regions where flood losses concentrate. Elsewhere, flood-specific perception studies report estimates only for the places where respondents were sampled, using instruments that vary across studies and limit comparability (S. P. Panda & Sethy, 2016; Sherly et al., 2019). We are not aware of national-scale estimates of flood risk perception for South Asia, where flood exposure and flood mortality are concentrated. Other Indian studies have examined climate risk perception and adaptation within particular regions (Singh et al., 2022), but none has produced national coverage, and none has addressed flood risk specifically. Empirical analyses of risk–perception misalignment have been conducted primarily in Europe and North America (Hunt et al., 2023; Khan et al., 2025; Mol et al., 2020; Palazzoli et al., 2025), with recent work beginning to extend beyond Western contexts (Xia et al., 2025). Work in the Global South remains localized (Rana & Routray, 2016), and India in particular is largely unstudied.

The Risk Analysis-Perception (RAP) framework (Marlon et al., 2025) offers a systematic way to quantify such misalignments between assessed and perceived flood risk, and has been applied to heat health risk in the United States, where it revealed substantial under-perception concentrated in Appalachia and the Pacific Northwest. Here, we apply it to flood risk in India, where floods differ from heat in spatial extent, forecast lead times, protective options, and the role of physical infrastructure in shaping exposure and perception. Using a nationally representative survey of Indian adults (N = 10,704), we develop a Multilevel Machine Learning with Poststratification (MMLP) approach to produce the first national-scale flood risk perception map for India at the district level. MMLP replaces the first-stage regression of poststratification with a machine learning classifier, following autoMrP (Broniecki et al., 2022), and weights the resulting predictions by each district's census population so that estimates extend to districts with few survey respondents. We then calculate alignment gaps between perceived and assessed risk across 633 districts to identify where the two diverge most sharply. Going beyond the map, we ask what explains the gap, testing district-level environmental, socioeconomic and information-environment covariates against administrative structure. The map identifies the populations most in need of targeted communication, and the attribution analysis indicates the level at which that effort is best organized.

2 Results

2.1 Assessed flood risk

The assessed flood risk map reveals a strong geographic pattern reflecting both well-known flood-prone regions and finer variation within states and river basins (Figure 1, Panel a & b). High assessed risk is concentrated along the Ganges and Brahmaputra river systems, low-lying floodplains in Bihar and Assam, and coastal regions in the western and southern parts of the country. The district-level assessed risk index, built from historical flood counts spanning 1969 to 2019 (India Meteorological Department, 2022), ranges from 0 to 100, with a national mean of 38 and a median of 37, indicating that most districts sit near the middle of the range rather than at either extreme. This index provides the physical baseline against which perceived risk is compared.

2.2 Perceived flood risk

The estimated national share of adults who perceive flooding as a risk is 59%. District-level estimates show substantial spatial variation in that share, ranging from 23% to 87% across the country (Figure 1, Panel c & d). Perceived flood risk is highest in the union territory of Dadra & Nagar Haveli and Daman & Diu, along with Himachal Pradesh, Tripura, Punjab, and Jammu & Kashmir, followed by Haryana, Meghalaya, Delhi, Odisha, Gujarat, Uttarakhand, and Uttar Pradesh. In contrast, perceived flood risk is lowest in the southern states of Telangana, Andhra Pradesh, and Karnataka. These estimates were validated against weighted survey aggregates, with a mean absolute error (MAE) of 4.31 percentage points at the state level and 9.47 percentage points at the district level. Both errors are small relative to the 23–87% spread across districts, indicating that the model recovers the geographic pattern of flood worry rather than averaging it away.

Underlying these district estimates is a gradient boosting classifier fit to individual survey responses, which showed the highest accuracy and F1 values (0.600 and 0.658, respectively) among the four candidates compared (Table 1). Classification performance in this range is expected at the individual level, where attitudinal responses are inherently noisy. Poststratification then aggregates these individual-level predictions to the district and state level. SHapley Additive exPlanations (SHAP) analysis (Lundberg & Lee, 2017) reveals that the strongest predictors in the classifier are spatial features (e.g., the spatially lagged worry rate), which capture clustering in flood worry, followed by individual demographic variables, particularly urban residence and gender. This ordering indicates that flood worry is not random and is shaped more by place than by demographic profile. The full SHAP values for each covariate are reported in Appendix B.

Table 1: Machine learning model performance on held-out test set

Classifier	Accuracy	AUC	F1	Precision	Recall
Random Forest	0.538	0.551	0.608	0.565	0.658
Gradient Boosting	**0.600**	0.622	**0.658**	0.616	**0.707**
Logistic Regression	0.516	0.541	0.546	0.558	0.535
LightGBM	0.588	**0.624**	0.618	**0.624**	0.612

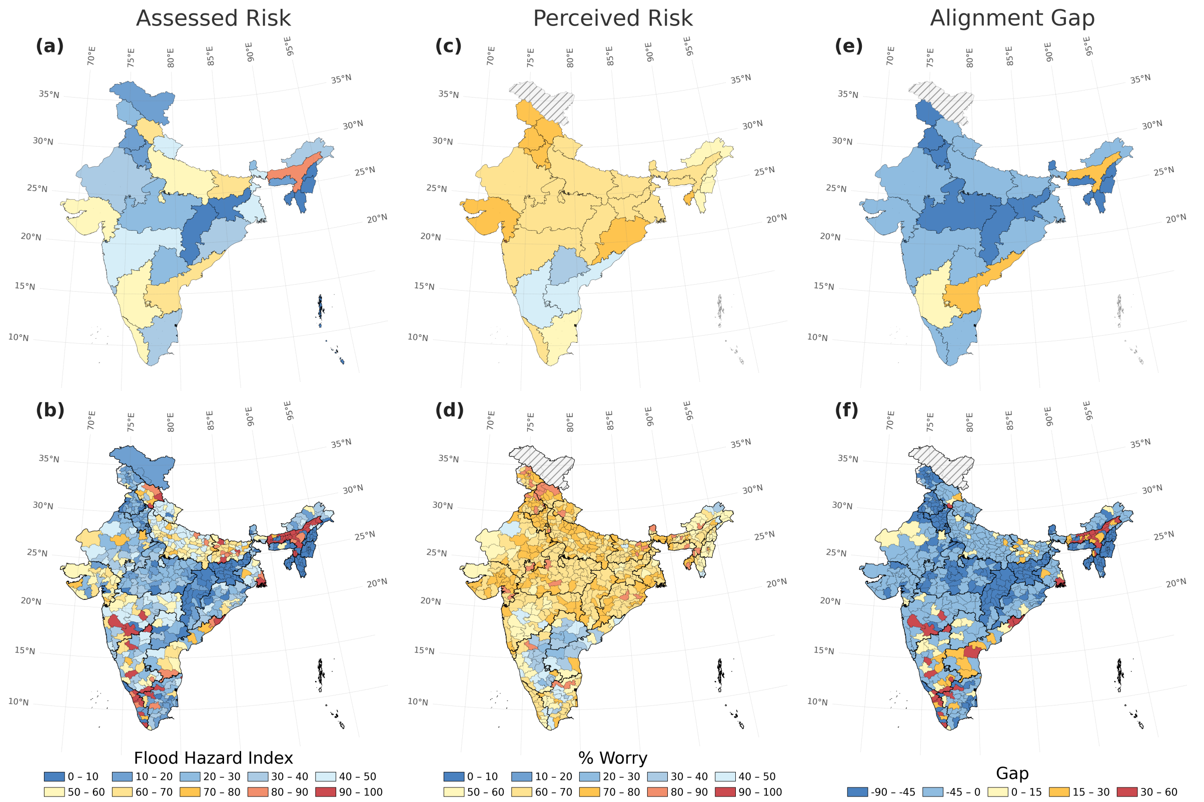

Figure 1: Maps showing assessed (left panel) and perceived (middle panel) flood risk with the alignment gap (right panel) at state (top row) and district (bottom row) levels.

2.3 Gaps between perceived and assessed flood risk

The gap between assessed and perceived flood risk reveals that public worry does not consistently track physical hazard across India (Figure 1, Panel e & f). The gap is calculated as normalized assessed risk minus perceived risk and expressed in percentage points, so that positive values indicate under-perception and negative values indicate over-perception. Across all 633 districts, the mean gap is -27.5 percentage points, indicating that nationally perceived risk tends to exceed assessed risk, though this aggregate masks pronounced regional heterogeneity. The gap ranges from -87.4 percentage points in the most over-perceiving districts to $+58.7$ percentage points in the most under-perceiving districts, with a standard deviation of 29.8 percentage points. Gaps exceed 30 percentage points in 54.5% of districts, well beyond the 9.47 percentage-point district-level error of these estimates. Because perceived risk is a population share while assessed risk is a normalized hazard index, the level of the gap depends in part on the scaling of the index, whereas the spatial pattern of divergence does not. Across four alternative rescalings of the flood count, the state share of variance in the gap stays between 55.5% and 60.0% (see Appendix E).

The resulting gap map reveals spatially clustered mismatches rather than random variation. Only a handful of states show net under-perception, with average gaps above zero despite high assessed flood exposure, most pronounced in Assam, while over-perception is spread broadly across northern states such as Punjab, Haryana, and Jammu & Kashmir, central states such as Madhya Pradesh, Chhattisgarh, and Jharkhand, and northeastern states other than Assam. Figure 2 shows the districts and states where assessed risk is high but perceived risk remains low. Where this mismatch is largest, the risk is not the hazard itself but the gap between what communities expect and what the floodplain delivers.

2.4 Typology of risk–perception alignment

To synthesize these patterns, we classify the 633 districts by whether their assessed and perceived risk fall above or below the district-level medians (flood count of 23; perceived risk of 67.3%), yielding four quadrants (Figure 3; the full per-state breakdown is reported in Appendix C). The classification typology uses the underlying flood count for assessed risk rather than the normalized index, which is capped at

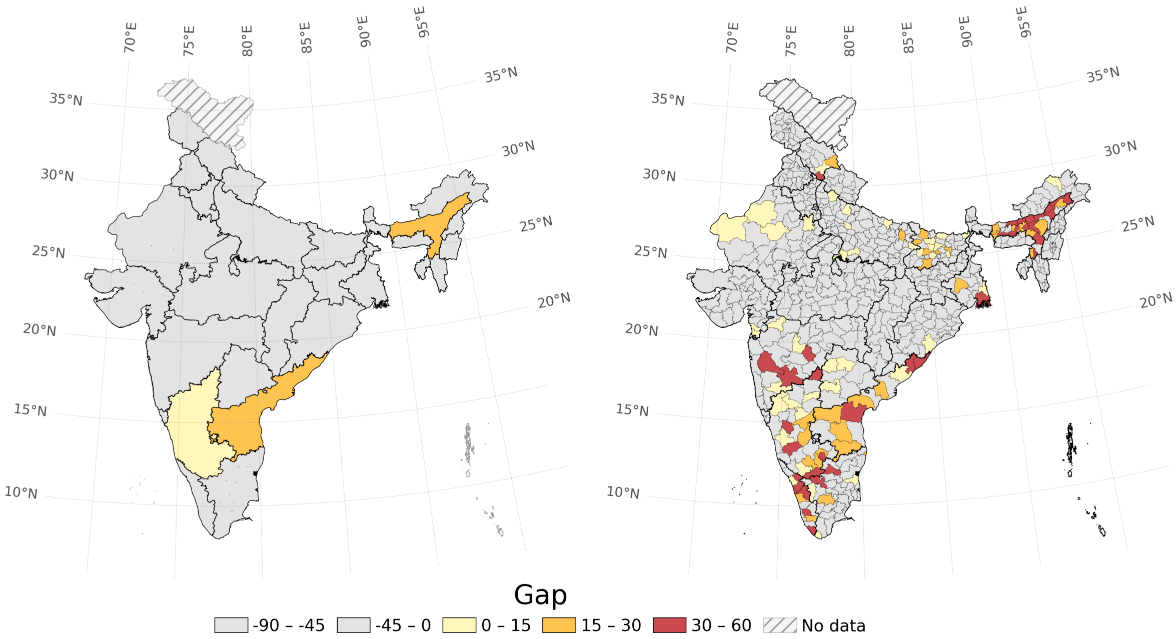

Figure 2: States (left) and districts (right) with high assessed but low perceived flood risk; all other areas are shown in grey.

its 95th percentile, so that the most flood-affected districts remain distinguishable from one another. Because assessed and perceived risk are nearly uncorrelated across districts ($r \approx -0.02$), a median split places close to a quarter of districts in each quadrant by construction. The substantive result therefore lies in which states fall where, not in the quadrant sizes.

Quadrant I, high assessed and low perceived risk (160 districts, 25.3%), is the most dangerous misalignment. Ranked by mean gap among each state's Quadrant I districts, it is concentrated in Assam, Kerala, and Andhra Pradesh, with gaps reaching 58.7 percentage points. Quadrant II, aligned under high exposure (149, 23.5%), is concentrated by within-state share in Himachal Pradesh, Bihar, and Uttarakhand, where repeated flooding appears to sustain awareness. Quadrant III, low assessed but high perceived risk (168, 26.5%), falls in Delhi, Tripura, and Haryana, and Quadrant IV, low on both (156, 24.6%), in Puducherry, Nagaland, and Mizoram. Where under-perception dominates, the lever is communication and early warning; where over-perception dominates, improving institutional trust may be more important than awareness campaigns.

2.5 What explains the gap

To understand where the alignment gap comes from, we modeled it as a function of district environmental, socioeconomic, and information-environment covariates alongside state fixed effects (see Appendix D). Two district-level covariates are statistically significant: night-time light ($p = 0.006$), where higher radiance shifts the gap toward over-perception, and flood-news article count ($p = 0.019$), where heavier coverage shifts it toward under-perception. Every other standardized coefficient's confidence interval crosses zero, and because the news covariates are median-imputed for the majority of districts lacking sufficient coverage (see Appendix D), both associations should be read with caution. The full model coefficients are reported in Appendix D.

These district-level gradients explain little of the gap overall. The gap is instead overwhelmingly organized at the state scale. State fixed effects alone account for 57.9% of the variance, whereas the ten district-level covariates jointly account for only 20.0%, and adding them on top of state fixed effects raises explained variance by less than one percentage point (Table 2). Across the full model, $R^2 = 0.588$ (adjusted $R^2 = 0.559$; robust Wald $F(42, 590) = 112.31$, $p < 0.001$).

This organization is not an artifact of the perception model, whose spatial lag features average over adjacent districts irrespective of state membership, since smoothing of that kind would blur variation across state borders rather than align with them. Nor is it an artifact of the partition itself. River basins, the natural physical-geography alternative, explain less than half as much of the gap as states do and add

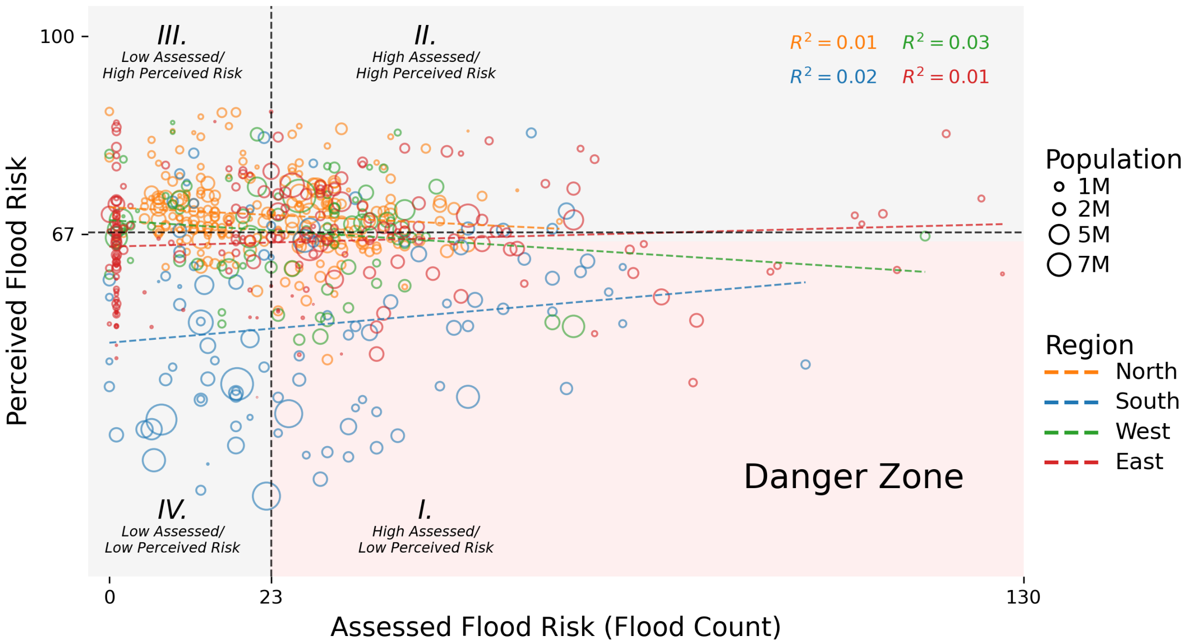

Figure 3: Assessed versus perceived flood risk across districts. Each point is a district, scaled by population and colored by region. Quadrants are defined by district-level medians: Quadrant I (high assessed, low perceived), II (high, high), III (low, high), and IV (low, low). Dashed lines are region-wise linear fits, with their R^2 values shown.

Table 2: Variance in the alignment gap explained by each specification ($N = 633$ districts).

Specification	R^2	adj. R^2
Covariates only	0.200	0.187
State fixed effects only	0.579	0.556
Covariates + state fixed effects	0.588	0.559

nothing once state is controlled for, and state fixed effects outperform all of 2,000 random partitions of equal resolution. Spatial autocorrelation in the gap, strong in the residuals of the covariate-only model, is no longer detectable once state fixed effects are included. The decomposition therefore indicates that misalignment is generated at the state scale rather than the individual district, so communication tailored to district covariates alone is unlikely to close it. Appendix D reports these checks in full, covering the river-basin comparison, the random-partition test, and the residual spatial autocorrelation.

3 Discussion

India's first national-scale flood risk perception map reveals that public worry does not merely track physical hazard. Although earlier localized studies could only hint at this fragmentation (S. P. Panda & Sethy, 2016; Sherly et al., 2019), our national map shows that it is not idiosyncratic, but systematic and geographically structured. The mismatch is also larger than the uncertainty in our estimates. Alignment gaps exceed 30 percentage points in 54.5% of districts, well beyond the district-level error of 9.47 percentage points, so the direction and scale of the mismatch hold even where its exact magnitude in a given district does not. Because the mismatch is both real and spatially organized, it identifies where targeted risk communication could do the most to close the gap.

We translate these findings into action through four risk–perception alignment quadrants (Figure 3), each with a different profile of assessed and perceived risk that calls for a different administrative response. The most concerning misalignment is Quadrant I, where assessed risk is high but perceived risk is low. It tends to arise where chronic exposure has been normalized, where protective infrastructure such as embankments or dams fosters a false sense of security, or where there have been few or no recent extreme events, so that perceptions stay low even as structural vulnerability remains high (Aerts et al., 2018; Kundzewicz et al., 2018; Lechowska, 2018). Survey evidence from Kerala, one of the states where under-perception is most pronounced in our results, finds that greater awareness of flood risk is associated with lower trust in government preparedness (Chandran MC et al., 2026), consistent with low perceived risk and confidence in official protection travelling together. Under-perception here reduces household preparedness and slows responses to early warnings, increasing the likelihood of severe impacts when large floods occur (Aerts et al., 2018; Jongman et al., 2015). Communication that emphasizes latent vulnerabilities, infrastructure limits, and compound risks is therefore better matched to these districts than communication reflecting historical experience alone (Tullos, 2018).

In Quadrant II, perceived and assessed risk align under high exposure, typically in regions of recent or repeated damaging floods. Awareness is therefore not the binding constraint in these districts, though alignment does not guarantee adaptive capacity. High awareness can coexist with limited resources, institutional constraints, or adaptation fatigue (Aerts et al., 2018; Jongman et al., 2015), so interventions should focus less on raising awareness and more on enabling action through infrastructure, social protection, and locally appropriate adaptation (Cano Pecharroman & Hahn, 2024; Jongman et al., 2015). In Quadrant III, where perceived risk runs ahead of assessed risk, elevated worry may reflect recent anomalous events, media amplification, or local stressors such as waterlogging and urban drainage failures that large-scale metrics miss (Kellens et al., 2013). Such concern is not necessarily misinformed, yet sustained worry over threats that are unlikely to materialize can erode institutional trust and impose a chronic psychological burden (Savari et al., 2025). Effective communication in these districts would acknowledge lived experience while clarifying the actual magnitude of risk.

Quadrant IV districts are aligned on both counts, but may not remain so permanently. Land-use change, urban expansion, and shifting precipitation can raise exposure over time (Rentschler et al., 2023; Winsemius et al., 2016). Warming adds hazards with little historical precedent, as when a glacial collapse on the Nepal–Tibet border in August 2026 sent floodwaters through valleys within minutes (The New York Times, 2026); events of this kind escape both assessed measures built from past flood records and perceptions anchored in lived experience. Maintaining baseline awareness and integrating flood risk into development planning can maintain alignment as conditions change. By showing where under-perception, alignment, or over-perception dominates, the RAP framework gives disaster managers a basis for matching communication and adaptation strategies to the kind of misalignment a region actually faces.

While flood hazard varies district by district, we find that in India the alignment gap is structured more strongly by state than by district conditions. Once state structure is accounted for, district-level covariates spanning climate, hydrology, education, vulnerability, and the local information environment explain little of the remaining variation. The flood case extends the RAP framework by identifying the administrative scale at which misalignment is organized, a question the original heat-risk analysis did not test (Marlon et al., 2025). That organization plausibly follows from how flood risk is governed and communicated in India. Under the Disaster Management Act, state authorities set disaster policy and plans for their state and fix the standards of relief that follow a flood, while embankments and drainage are the responsibility of state water departments (Government of India, 2005). Public communication is similarly state-bound, since news markets are organized by language and language boundaries broadly follow state boundaries. Each would generate structure at the scale we observe. Messaging designed district by district may therefore have limited reach if the expectations it addresses are shaped at the state scale.

This pattern has parallels elsewhere. Across the contiguous United States, mapped flood risk perception aligns only weakly with flood exposure (Allan et al., 2020). Housing markets there do not fully capitalize publicly available flood-map information, and the discount that does appear is larger in states that mandate flood-risk disclosure (Hino & Burke, 2021), so perception-relevant behaviour varies with state policy in a setting where that policy variation can be measured. Recent work in China has mapped climate risk perception against assessed exposure at provincial and city scales, reporting growing regional disparities between the two (Xia et al., 2025), though it treated that spatial structure descriptively rather than testing the scale at which it is generated. Our results are consistent with these, and extend them by asking whether the structure is administrative in origin. We cannot establish which channel is responsible, because data on state-level policy and public communication in India are not available. The mechanisms described above therefore remain hypotheses.

These findings have direct implications for how flood-risk resources are allocated in India. Targeting flood preparedness on hazard exposure alone assumes that high-risk populations recognize their risk. Our results show that this assumption fails in a substantial number of districts. Coupling perception data with hazard maps could shift targeting toward populations whose preparedness gaps are largest, particularly the under-perception zones identified in Quadrant I. Beyond India, the framework provides a transferable instrument for any national context in which flood exposure is well measured, but public risk perception is not. Periodic perception surveys would allow these changes in gaps to be tracked as exposure, awareness, and demographics shift.

The framework opens several directions as new data become available. Repeating the survey, particularly after major floods, would turn the map into a record of how perception moves and would distinguish stable attitudes from event-driven shifts. Extending the assessed measure from how often floods occur to how much damage they cause would add a further dimension to the alignment gap. The poststratification step depends on the census data, which for these estimates is the 2011 Census. Counts from a newer census would refresh the population weights and give an updated picture of how flood risk perception is distributed across India today. Each of these builds on the same framework, so the map can be updated as India's flood and demographic records grow.

Perception data of this kind have not previously been available for India at a resolution useful to planners. Producing them required extending poststratification with a machine learning first stage, yielding district-level estimates that hold up against weighted survey aggregates and extend to districts no survey reached. The same approach applies wherever flood hazard is well measured but public perception is not.

4 Methods

We estimated spatial patterns of perceived flood risk across India using survey-based measures and compared them with assessed flood risk to identify areas of alignment and misalignment. Our analysis integrated individual-level survey data and district-level environmental and socioeconomic indicators, including AlphaEarth satellite embeddings, within the RAP framework.

4.1 Assessed flood risk

For assessed flood risk, we used the district-level flood count from the Climate Hazards and Vulnerability Atlas of India by the India Meteorological Department, Ministry of Earth Sciences (India Meteorological Department, 2022), which records flood counts from 1969 to 2019 for all districts. We capped the raw flood count at its 95th percentile, divided it by that percentile, and multiplied by 100, giving a 0–100 index in which districts at or above the 95th percentile take the maximum value. Perceived risk is a population share, so placing assessed risk on the same 0–100 scale allows gaps between the two to be reported in percentage points. This index was used throughout the gap maps.

4.2 Survey data for perceived flood risk

We used data from the Climate Change in the Indian Mind (CCIM) survey conducted by the Yale Program on Climate Change Communication (YPCCC) between December 2024 and February 2025, comprising a nationally representative sample of 10,704 Indian adults. Individual-level covariates included gender, age, urbanicity, and caste. Detailed information on the survey, geographic coverage, variable coding, and demographic distributions is provided in Appendix A.

4.3 Data harmonization and reporting universe

Population weights were based on the 2011 Census of India, the most recent available. We harmonized 2011 Census units to contemporary (2023) survey and geographic boundaries using state- and district-level crosswalks that accounted for boundary changes, name-spelling differences, and merged or newly created districts. Of the 640 districts in the 2011 Census, four island districts (Andaman & Nicobar and Lakshadweep) were excluded for lack of complete census and hazard coverage, and three further districts had no counterpart in the boundary crosswalk, yielding the 633-district reporting universe used throughout, including the gap maps, the quadrant typology, and the gap-attribution regression. Survey respondents fell in 596 of these 633 districts. District-level population counts were obtained from a 2023 district shapefile covering 733 district polygons.

4.4 District-level covariates

District-level covariates captured environmental context, socioeconomic conditions, physical exposure, and experiential signals relevant to perception. They included the share of residents with higher-secondary education or above, the CEEW climate vulnerability index, climate and hydrological variables, proxies for human activity, AlphaEarth satellite embeddings, and news-media sentiment, all harmonized to a common spatial framework. We additionally constructed spatial lag covariates, computed as weighted averages of neighboring districts' flood worry and selected environmental indicators, so that the model could draw on conditions in neighboring districts as well as within each district (details in Appendix B).

Table 3 summarizes the covariates used in this study, their sources, and their native resolutions.

Data	**Source**	**Year**	**Data Type**	**Remarks**
District-Level Physical & Environmental Covariates				
Average Precipitation	ERA5 Reanalysis v5.0 (Hersbach et al., 2020)	2024	Continuous	Daily total precipitation (min, mean, max); aggregated to district level
Average Temperature	ERA5 Reanalysis v5.0 (Hersbach et al., 2020)	2024	Continuous	Daily temperature (min, mean, max); aggregated to district level
Night Time Light (DNB Radiance)	Earth Observation Group, Univ. of Colorado Mines via GEE (Gorelick et al., 2017)	2024	Continuous	Average Day/Night Band radiance (mean, median); 463.8 m resolution; aggregated to district level
AlphaEarth Embeddings	Google Earth Engine / DeepMind (Brown et al., 2025)	2024	Continuous	64 analysis-ready embeddings (min, mean, max, percentiles); 10 m resolution; aggregated to district level
Flow Accumulation	HydroSHEDS via GEE (Lehner et al., 2008)	2024	Continuous	Number of upstream pixels draining into each cell; summed to district level
News Media Sentiment	GDELT / Global Knowledge Graph (Leetaru & Schrodt, 2013)	2024	Continuous	Tone, polarity, and emotion of news coverage; natively at district level
District-Level Socioeconomic & Vulnerability Covariates				
Climate Vulnerability Index	CEEW (A. Mohanty & Wadhawan, 2021)	2021	Continuous	Product of exposure and sensitivity divided by adaptive capacity; standardized to $[-2, 2]$
Higher Education	Census of India	2011	Continuous	Percentage of the population who attended higher secondary school or above; standardized to $[-2, 2]$
Individual-Level Survey Covariates				
Age	Survey data	—	Continuous	Four groups: 18–29, 30–44, 45–59, 60+
Gender	Survey data	—	Categorical	Male and Female
Caste	Survey data	—	Categorical	Scheduled Castes/Tribes and Other Castes
Urbanicity	Survey data	—	Categorical	Rural and Urban

Table 3: Survey and covariate data used in this study, organized by type. GEE: Google Earth Engine; ERA5: Fifth Generation ECMWF Atmospheric Reanalysis; CEEW: Council on Energy, Environment and Water; DNB: Day/Night Band. All district-level physical covariates were aggregated from their native resolutions to administrative district boundaries.

All gridded covariates were aggregated to district boundaries by spatially averaging the cells falling within each district, except flow accumulation, which was summed. The CEEW vulnerability index and the higher-secondary education share were standardized to a $[-2, 2]$ range by centering at the mean, scaling by the standard deviation, and capping values beyond two standard deviations. Source products, catalog identifiers, native resolutions, and the nighttime-light, population-density and elevation context layers are given in Appendix A.

4.5 Modeling perceived flood risk

We modeled perceived flood risk using MMLP, which builds on multilevel regression with poststratification (MrP), a two-stage approach known to outperform conventional methods in areas with sparse samples (Caughey & Warshaw, 2019; Howe et al., 2015; Pacheco, 2011), but replaces its first-stage regression with a Machine Learning (ML) classifier. We compared four ML classifiers (Random Forest, Gradient Boosting, Logistic Regression, and LightGBM) and selected the best-performing one (see Validation, Section 4.6). Hyperparameters were selected via five-fold cross-validated grid search, and the train–test split was spatially stratified to prevent spatial data leakage.

The selected classifier was then used to estimate the probability of perceiving flood risk for each demographic-geographic group from individual survey responses (gender, age group, caste, and urbanicity, with their full interaction) and the district-level covariates described above, matched to respondents by district. Poststratification then weighted these fitted probabilities by each group's 2011 Census population share, extending estimates from the 596 districts with survey coverage to all 633 districts with census data and yielding perceived-risk estimates for the 2024–2025 period.

For geography a, the estimated share of adults perceiving flood risk is

$$\hat{y}_a = \frac{\sum_{g \in a} \hat{p}_g N_g}{\sum_{g \in a} N_g}, \tag{1}$$

where g indexes demographic-geographic cells (defined by the interaction of gender, age group, caste, and urbanicity within geography a), $\hat{p}_g$ is the classifier's fitted probability of flood-risk perception for cell g, and N_g is the 2011 Census population count for that cell.

Poststratification reweights sparse or unrepresentative cells in the survey sample toward their true population shares, allowing district-level estimates in low-response areas to borrow strength from the fitted model rather than relying on raw survey means.

4.6 Validation

We validated the classifier that generates individual-level predictions and, separately, the poststratified estimates that follow from it.

For the classifier, we compared the four candidates on a spatially blocked held-out test set. Because neighboring districts resemble one another, training and testing on adjacent districts can make a model appear more accurate than it is (see Appendix B), so districts were assigned to 250 km × 250 km grid cells by centroid and 13 of 75 cells (17%) were withheld, ensuring no test district shares a block with a training district. This produced an 83.5%/16.5% split of 8,936 and 1,768 respondents (Figure 4). Classifiers were compared on accuracy and F1, which weighs recall alongside precision, because the analysis required identifying flood-worried respondents across the full population rather than minimizing false positives.

For the poststratified estimates, we compared modeled shares against weighted survey aggregates and report mean absolute error in percentage points, computed for districts with at least 50 respondents ($n = 20$) and states with at least 500 ($n = 9$).

4.7 Typology of risk–perception alignment

We classified districts into four quadrants by whether their assessed and perceived risk fell above or below the district-level medians (flood count 23; perceived risk 67.3%), chosen over means because flood count is right-skewed. The typology used the raw, unclipped flood count rather than the normalized index, so that the extreme high-flood districts capped by the 95th percentile clip remained distinguishable. To select the states reported for each quadrant, we ranked them by severity for Quadrant I (mean percentage-point gap among its Quadrant I districts) and by within-state share for Quadrants II–IV, restricting to states with at least three districts in the quadrant (Appendix C).

4.8 Gap attribution model

To understand what explains the gap between assessed and perceived flood risk, we regressed the district-level gap on ten standardized covariates and state fixed effects, using ordinary least squares. The covariates spanned hydrology and climate, socioeconomic conditions, and the local news environment.

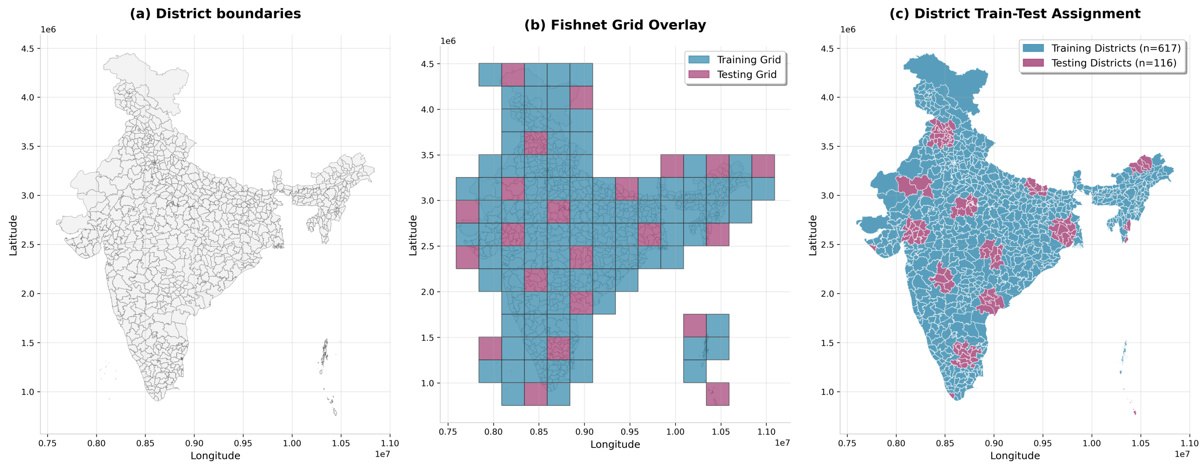

Figure 4: Spatially blocked train–test split using 250 km × 250 km grid cells. Panel (c) colours all 733 polygons of the 2023 district shapefile by the block they fall in, including polygons in districts with no survey respondents.

To separate within-state variation from state-level structure, we estimated three nested specifications: covariates only, state fixed effects only, and the full model (see Appendix D).

For district i in state s, the model is

$$\text{gap}_i = \alpha + \sum_k \beta_k \, z_{ki} + \gamma_{s(i)} + \varepsilon_i, \tag{2}$$

where z_{ki} is the standardized value of covariate k, $\gamma_{s(i)}$ is a state fixed effect (dummy-coded, with Andhra Pradesh, the alphabetically first state, as the omitted reference category), and ε_i is the residual.

Acknowledgements

Pratyush Tripathy was supported by National Aeronautics and Space Administration (NASA) under Grant No. 80NSSC25K0392 issued through their Future Investigators in NASA Earth and Space Science and Technology (FINESST) program. The authors acknowledge the support of the Institute for Geospatial Understanding through an Integrative Discovery Environment (I-GUIDE) and the John D. and Catherine T. MacArthur Foundation. The authors used Claude Opus 5 to assist with analysis code and manuscript editing, and take full responsibility for the published content.

Data availability

Individual-level responses from the Climate Change in the Indian Mind survey are not publicly deposited and are available from the Yale Program on Climate Change Communication on request. All district-level estimates and covariates needed to reproduce the reported results are publicly available at https://github.com/YCGS-lab/india-flood-risk-perception-gap.

Code availability

The analysis code needed to reproduce the reported results is publicly available at https://github.com/YCGS-lab/india-flood-risk-perception-gap.

Competing interests

The authors declare no competing interests.

Author contributions

P.T., S.U., O.M.A., E.S., D.P., E.G., and J.M. designed and performed research; A.L. and J.M. coordinated the project and A.L. and J.T. acquired the data; P.T., S.U., O.M.A., E.S., D.P., and E.G. analyzed data; and P.T., S.U., O.M.A., E.S., D.P., E.G., and J.M. wrote the paper, with input from J.T. and A.L.

References

Aerts, J. C. J. H., Botzen, W. J. W., Clarke, K. C., Cutter, S. L., Hall, J. W., Merz, B., Michel-Kerjan, E., Mysiak, J., Surminski, S., & Kunreuther, H. (2018). Integrating human behaviour dynamics into flood disaster risk assessment. *Nature Climate Change*, *8*, 193–199. https://doi.org/10.1038/s41558-018-0085-1

Allan, J. N., Ripberger, J. T., Wehde, W., Krocak, M., Silva, C. L., & Jenkins-Smith, H. C. (2020). Geographic distributions of extreme weather risk perceptions in the United States. *Risk Analysis*, *40*(12), 2498–2508. https://doi.org/10.1111/risa.13569

Broniecki, P., Leemann, L., & Wüest, R. (2022). Improved multilevel regression with poststratification through machine learning (automrp). *The Journal of Politics*, *84*(1), 597–601.

Brown, C. F., Kazmierski, M. R., Pasquarella, V. J., Rucklidge, W. J., Samsikova, M., Zhang, C., Shelhamer, E., Lahera, E., Wiles, O., Ilyushchenko, S., et al. (2025). Alphaearth foundations: An embedding field model for accurate and efficient global mapping from sparse label data. *arXiv preprint arXiv:2507.22291*.

Bubeck, P., Botzen, W. J. W., & Aerts, J. C. (2012). A review of risk perceptions and other factors that influence flood mitigation behavior. *Risk Analysis*, *32*(9), 1481–1495.

Cano Pecharroman, L., & Hahn, C. (2024). Exposing disparities in flood adaptation for equitable future interventions in the USA. *Nature Communications*, *15*, 8333. https://doi.org/10.1038/s41467-024-52111-0

Caughey, D., & Warshaw, C. (2019). Public opinion in subnational politics.

Chandran MC, S., Chandran, R., Rao Sahib, P., & Achuthan, K. (2026). Flood risk perception and water infrastructure: Understanding public response to climate change. *Natural Hazards*, *122*(5), 207.

Dasgupta, S., Barua, A., Murthy, I. K., Borgohain, P. L., Baghel, T., Sankhyayan, P., Vidya, S., Narwal, H., Jan, A., Vyas, S., Luniwal, Y., Ghosh, S., Cheranda, T. M., Alam, M. K., Mathew, S., & Pradeep, M. S. (2024). *District-level climate risk assessment for india: Mapping flood and drought risks using ipcc framework* (Report). Department of Science, Technology, Government of India, Swiss Agency for Development, and Cooperation (SDC), Embassy of Switzerland. New Delhi, India.

Dhiman, R., VishnuRadhan, R., Eldho, T., & Inamdar, A. (2019). Flood risk and adaptation in Indian coastal cities: Recent scenarios. *Applied Water Science*, *9*(1), 5.

Farr, T. G., Rosen, P. A., Caro, E., Crippen, R., Duren, R., Hensley, S., Kobrick, M., Paller, M., Rodriguez, E., Roth, L., Seal, D., Shaffer, S., Shimada, J., Umland, J., Werner, M., Oskin, M., Burbank, D., & Alsdorf, D. (2007). The shuttle radar topography mission. *Reviews of Geophysics*, *45*(2), RG2004. https://doi.org/10.1029/2005RG000183

Gorelick, N., Hancher, M., Dixon, M., Ilyushchenko, S., Thau, D., & Moore, R. (2017). Google Earth Engine: Planetary-scale geospatial analysis for everyone. *Remote sensing of Environment*, *202*, 18–27.

Government of India. (2005). The disaster management act, 2005. https://www.indiacode.nic.in/handle/123456789/2045

Grothmann, T., & Reusswig, F. (2006). People at risk of flooding: Why some residents take precautionary action while others do not. *Natural Hazards*, *38*(1-2), 101–120. https://doi.org/10.1007/s11069-005-8604-6

Hersbach, H., Bell, B., Berrisford, P., Hirahara, S., Horányi, A., Muñoz-Sabater, J., Nicolas, J., Peubey, C., Radu, R., Schepers, D., et al. (2020). The ERA5 global reanalysis. *Quarterly journal of the royal meteorological society*, *146*(730), 1999–2049.

Hino, M., & Burke, M. (2021). The effect of information about climate risk on property values. *Proceedings of the National Academy of Sciences*, *118*(17), e2003374118. https://doi.org/10.1073/pnas.2003374118

Howe, P. D., Marlon, J. R., Wang, X., & Leiserowitz, A. (2019). Public perceptions of the health risks of extreme heat across US states, counties, and neighborhoods. *Proceedings of the National Academy of Sciences*, *116*(14), 6743–6748. https://doi.org/10.1073/pnas.1813145116

Howe, P. D., Mildenberger, M., Marlon, J. R., & Leiserowitz, A. (2015). Geographic variation in opinions on climate change at state and local scales in the USA. *Nature Climate Change*, *5*, 596–603. https://doi.org/10.1038/nclimate2583

Howe, P. D., Thaker, J., & Leiserowitz, A. (2014). Public perceptions of rainfall change in India. *Climatic Change*, *127*(2), 211–225.

Hunt, L., Williamson, M., & Hillis, V. (2023). Spatial (mis)alignment between climate-related risks and risk perceptions across the US. *Environmental Research Letters*, *18*(2), 021001. https://doi.org/10.1088/1748-9326/acb06c

India Meteorological Department. (2022). Climate hazards and vulnerability atlas of India [Accessed: 2026-03-09]. https://imdpune.gov.in/hazardatlas/index.html

Jacinth Jennifer, J., Saravanan, S., & Abijith, D. (2022). Integration of SAR and multi-spectral imagery in flood inundation mapping–a case study on Kerala floods 2018. *ISH Journal of Hydraulic Engineering*, *28*(sup1), 480–490.

Jain, G., Yang, W., Sarkar, S. K., Frazier, A. E., & Connor, D. S. (2025). CoSal: A remote sensing and machine learning framework for mapping coastal soil salinity trends around aquaculture in South Asia [Preprint, Research Square. https://doi.org/10.21203/rs.3.rs-6173117/v1].

Jongman, B., Winsemius, H. C., Aerts, J. C. J. H., Coughlan de Perez, E., van Aalst, M. K., Kron, W., & Ward, P. J. (2015). Declining vulnerability to river floods and the global benefits of adaptation. *Proceedings of the National Academy of Sciences*, *112*(18), E2271–E2280. https://doi.org/10.1073/pnas.1414439112

Kellens, W., Terpstra, T., & De Maeyer, P. (2013). Perception and communication of flood risks: A systematic review of empirical research. *Risk Analysis*, *33*(1), 24–49. https://doi.org/10.1111/j.1539-6924.2012.01844.x

Kellens, W., Zaalberg, R., Neutens, T., Vanneuville, W., & De Maeyer, P. (2011). An analysis of the public perception of flood risk on the belgian coast. *Risk Analysis*, *31*(7), 1055–1068.

Khan, M. A., Zia, A., Merrill, S. C., Koliba, C., & Balerna, J. (2025). Bridging the gap: Discrepancies between public flood risk perceptions and FEMA map designations in the United States. *Risk Analysis*, *45*(3), 542–562. https://doi.org/10.1111/risa.14219

Kumar, A., Mondal, S., & Lal, P. (2022). Analysing frequent extreme flood incidences in Brahmaputra basin, south asia. *Plos one*, *17*(8), e0273384.

Kundzewicz, Z. W., Hegger, D. L. T., Matczak, P., & Driessen, P. P. J. (2018). Flood-risk reduction: Structural measures and diverse strategies. *Proceedings of the National Academy of Sciences*, *115*(49), 12321–12325. https://doi.org/10.1073/pnas.1818227115

Lechowska, E. (2018). What determines flood risk perception? a review of factors of flood risk perception and relations between its basic elements. *Natural Hazards*, *94*(3), 1341–1366.

Lee, T. M., Markowitz, E. M., Howe, P. D., Ko, C.-Y., & Leiserowitz, A. A. (2015). Predictors of public climate change awareness and risk perception around the world. *Nature climate change*, *5*(11), 1014–1020.

Leetaru, K., & Schrodt, P. A. (2013). GDELT: Global data on events, location, and tone, 1979–2012. *ISA annual convention*, *2*(4), 1–49.

Lehner, B., & Grill, G. (2013). Global river hydrography and network routing: Baseline data and new approaches to study the world's large river systems. *Hydrological Processes*, *27*(15), 2171–2186. https://doi.org/10.1002/hyp.9740

Lehner, B., Verdin, K., & Jarvis, A. (2008). New global hydrography derived from spaceborne elevation data. *Eos, Transactions American Geophysical Union*, *89*(10), 93–94. https://doi.org/10.1029/2008EO100001

Lundberg, S. M., & Lee, S.-I. (2017). A unified approach to interpreting model predictions. In I. Guyon, U. V. Luxburg, S. Bengio, H. Wallach, R. Fergus, S. Vishwanathan, & R. Garnett (Eds.), *Advances in neural information processing systems* (Vol. 30). Curran Associates, Inc. https://proceedings.neurips.cc/paper_files/paper/2017/file/8a20a8621978632d76c43dfd28b67767-Paper.pdf

Marlon, J. R., Begotka, N., Preston, A., Steifel, M., Keenan, J. M., Inman, C., Malmin, N. P., Carman, J., Goddard, E., Kotcher, J., Maibach, E., Rosenthal, S. A., & Leiserowitz, A. (2025). Experience-driven perceptions misalign with assessed heat risk in the United States. *Nature Communications*, *17*(1), 909. https://doi.org/10.1038/s41467-025-67631-6

Mohanty, A., & Wadhawan, S. (2021, October). Mapping India's climate vulnerability – a district level assessment. https://www.ceew.in/sites/default/files/ceew-study-on-climate-change-vulnerability-index-and-district-level-risk-assessment.pdf

Mohanty, M. P., Mudgil, S., & Karmakar, S. (2020). Flood management in India: A focussed review on the current status and future challenges. *International journal of disaster risk reduction*, *49*, 101660.

Mol, J. M., Botzen, W. W., Blasch, J. E., & de Moel, H. (2020). Insights into flood risk misperceptions of homeowners in the Dutch river delta. *Risk Analysis*, *40*(7), 1450–1468.

Moody's Analytics. (2024, September). *An integrated approach to evaluate population exposure to inland and coastal flooding* (tech. rep.) (Accessed 2025). Moody's Corporation. https://www.moodys.com/web/en/us/insights/resources/an-integrated-approach-to-evaluate-population-exposure-to-inland-and-coastal-flooding.pdf

Nagamani, K., Mishra, A. K., Meer, M. S., & Das, J. (2024). Understanding flash flooding in the Himalayan region: A case study. *Scientific Reports*, *14*(1), 7060.

National Remote Sensing Centre (NRSC). (2023). *Flood affected area atlas of india (1998–2022): Satellite based study* (Technical Report) (Prepared for the National Disaster Management Authority (NDMA), Ministry of Home Affairs, Government of India. Version 1.0). Indian Space Research Organisation (ISRO), Department of Space, Government of India. Hyderabad, India.

National Water Informatics Centre. (2025). Basin boundary of major rivers of India [Accessed: 2026-08-23]. https://nwdp.nwic.gov.in/dataset/basin-cwc

Pacheco, J. (2011). Using national surveys to measure dynamic US state public opinion: A guideline for scholars and an application. *State Politics & Policy Quarterly*, *11*(4), 415–439.

Palazzoli, I., Puglisi, C., Binelli, C., Muttarak, R., & Ceola, S. (2025). Public perceptions of flood risk: Evidence from major 2023 events in Italy. *SSRN*. https://doi.org/10.2139/ssrn.5655176

Panda, S. P., & Sethy, K. M. (2016). Human perception and response to flood hazards: A case study of Baitarani basin in Odisha. *Int J Appl Res*, *2*(5), 511–516.

Panda, S. R., Mishra, S. P., Tripathy, J. K., & Barik, K. K. (2021). The failed resilience, grim water future, and salinity intrusion through GIS of Kendrapara coast, Odisha. *International Journal of Lakes and Rivers*, *14*(2), 161–181.

Raaijmakers, R., Krywkow, J., & van der Veen, A. (2008). Flood risk perceptions and spatial multi-criteria analysis: An exploratory research for hazard mitigation. *Natural hazards*, *46*(3), 307–322.

Rana, I. A., & Routray, J. K. (2016). Actual vis-à-vis perceived risk of flood-prone urban communities in Pakistan. *International Journal of Disaster Risk Reduction*, *19*, 366–378. https://doi.org/10.1016/j.ijdrr.2016.08.028

Ratna, R. S., Huang, J., & Beriwal, S. (2025, October). From storm to strength: Odisha's "zero casualty" model for community-centered disaster resilience [Accessed October 2025]. https://www.unescap.org/blog/storm-strength-odishas-zero-casualty-model-community-centered-disaster-resilience

Rentschler, J., Avner, P., Marconcini, M., et al. (2023). Global evidence of rapid urban growth in flood zones since 1985. *Nature*, *622*, 87–92. https://doi.org/10.1038/s41586-023-06468-9

Rentschler, J., Salhab, M., & Jafino, B. A. (2022). Flood exposure and poverty in 188 countries. *Nature communications*, *13*(1), 3527.

Roy, S., Debnath, P., & Mitra, S. (2023). Impact of climate disasters on railway infrastructure: Case study of northeast India. *Acadlore Trans. Geosci*, *2*(1), 33–45.

Sahani, R. K., Badiger, S., Samrat, A., & Krishnan, S. (2023). Flood frequency and flood intensity changes in the post embankment period in the Kosi sub-basin India: Impact of location, caste, and class on the flood vulnerability of the marginal communities. *Frontiers in Water*, *5*, 1017945.

Savari, M., Jafari, A., & Sheheytavi, A. (2025). Determining factors affecting flood risk perception among local communities in iran. *Scientific Reports*, *15*(1), 4076. https://doi.org/10.1038/s41598-025-88673-2

Sherly, M., Janadri, K. K., & Karmakar, S. (2019). Fuzzy cognitive mapping of flood risk perception and adaptive capacity of slum communities over the most flood-prone city in India. *4th IMA International conference on Flood Risk (IMA 2019), Swansea University, UK*.

Singh, N. P., Anand, B., Srivastava, S., Kumar, N., Sharma, S., Bal, S., Rao, K., & Prabhakar, M. (2022). Risk, perception and adaptation to climate change: Evidence from arid region, India. *Natural Hazards*, *112*(2), 1015–1037.

Slovic, P., Finucane, M. L., Peters, E., & MacGregor, D. G. (2004). Risk as analysis and risk as feelings: Some thoughts about affect, reason, risk, and rationality. *Risk Analysis*, *24*(2), 311–322. https://doi.org/10.1111/j.0272-4332.2004.00433.x

Tellman, B., Sullivan, J. A., Kuhn, C., Kettner, A. J., Doyle, C. S., Brakenridge, G. R., Erickson, T. A., & Slayback, D. A. (2021). Satellite imaging reveals increased proportion of population exposed to floods. *Nature*, *596*(7870), 80–86. https://doi.org/10.1038/s41586-021-03695-w

Terpstra, T. (2011). Emotions, trust, and perceived risk: Affective and cognitive routes to flood preparedness behavior. *Risk Analysis*, *31*(10), 1658–1675. https://doi.org/10.1111/j.1539-6924.2011.01616.x

Thaker, J., Smith, N., & Leiserowitz, A. (2020). Global warming risk perceptions in India. *Risk Analysis*, *40*(12), 2481–2497.

The New York Times. (2021). Glacier bursts in india, leaving more than 100 missing in floods [https://www.nytimes.com/2021/02/07/world/asia/india-glacier-flood-uttarakhand.html, accessed August 2026].

The New York Times. (2026). Flash floods devastate nepal–tibet border region [https://www.nytimes.com/live/2026/08/27/world/nepal-tibet-flash-floods, accessed August 2026].

Tripathy, P., & Malladi, T. (2022). Global flood mapper: A novel Google Earth Engine application for rapid flood mapping using Sentinel-1 SAR. *Natural hazards*, *114*(2), 1341–1363.

Tullos, D. (2018). How to achieve better flood-risk governance in the united states. *Proceedings of the National Academy of Sciences*, *115*(15), 3731–3734. https://doi.org/10.1073/pnas.1722412115

Vegad, U., Pokhrel, Y., & Mishra, V. (2024). Flood risk assessment for Indian sub-continental river basins. *Hydrology and Earth System Sciences*, *28*(5), 1107–1126.

Wachinger, G., Renn, O., Begg, C., & Kuhlicke, C. (2013). The risk perception paradox—implications for governance and communication of natural hazards. *Risk Analysis*, *33*(6), 1049–1065. https://doi.org/10.1111/j.1539-6924.2012.01942.x

Winsemius, H. C., Aerts, J. C. J. H., van Beek, L. P. H., et al. (2016). Global drivers of future river flood risk. *Nature Climate Change*, *6*, 381–385. https://doi.org/10.1038/nclimate2893

Xia, Z., Ye, J., Debnath, R., Dong, X., Xie, J., Xu, M., Tian, X., Marlon, J., Zhang, C., Yang, J., Constantino, S., & Liu, M. (2025). Growing climate change risk concerns with rising regional disparities in China. *npj Climate Action*, *4*, 78. https://doi.org/10.1038/s44168-025-00272-z

Appendix A Data sources

Appendix A.1 Survey data

The CCIM data include one nationally representative survey of Indian adults aged 18 and older, conducted from December 2024 to February 2025 ($N = 10{,}751$). Of these, 47 responses were removed due to missing data, yielding a final sample of 10,704 respondents. The survey was administered by CVoter in 12 languages. Respondents were drawn from 32 of India's 36 states and Union territories, and 596 of the 633 reporting-universe districts had at least one survey respondent; the remaining districts had no direct survey coverage. Because the post-stratification model produces an estimate for every geographic-demographic cell for which covariate data are available, predictions were nonetheless generated for all 633 districts, with districts lacking direct respondents borrowing strength from the fitted model rather than from local data.

The 633-district universe follows 2011 Census district boundaries, excluding four island districts (Andaman & Nicobar and Lakshadweep) and three districts without a counterpart in the boundary crosswalk; of the 633, a smaller subset met a minimum threshold of 50 respondents and were retained for district-level reliability reporting (see the main text, Methods/Validation, for the exact count and reliability threshold). The working shapefile contains 733 polygons, of which 725 match a 2011 Census district through the crosswalk. These 725 matched polygons resolve to the 633 districts of the reporting universe. Sixty-nine census districts were later split into two or more present-day (2023-boundary) districts, contributing 92 polygons beyond one per census district, and these split polygons are dissolved (geometries unioned, values averaged) into their parent census district rather than excluded. Ladakh, constituted in 2019, has no counterpart in the 2011 Census and is therefore absent from the crosswalk. Because assessed risk is derived directly from geographic hazard data independent of the survey crosswalk, it is plotted wherever available even for districts outside the 633-district reporting universe; perceived risk and the gap, which require a crosswalk match, are not. In the maps, polygons lacking data for a given panel are shown with a hatched pattern. The gap-attribution regression (Appendix D) is estimated on this same 633-district dissolved population.

The dependent variable is a dichotomized indicator of flood worry, coded one for respondents who report worry about flooding. Individual-level covariates included gender (male, female), age (18–29, 30–44, 45–59, 60+), caste (Scheduled Castes/Tribes, Other Castes), and urbanicity (urban, rural). Figure A5 shows the spatial distribution of survey respondents across India and the demographic distributions of gender, age, caste, and urban/rural location.

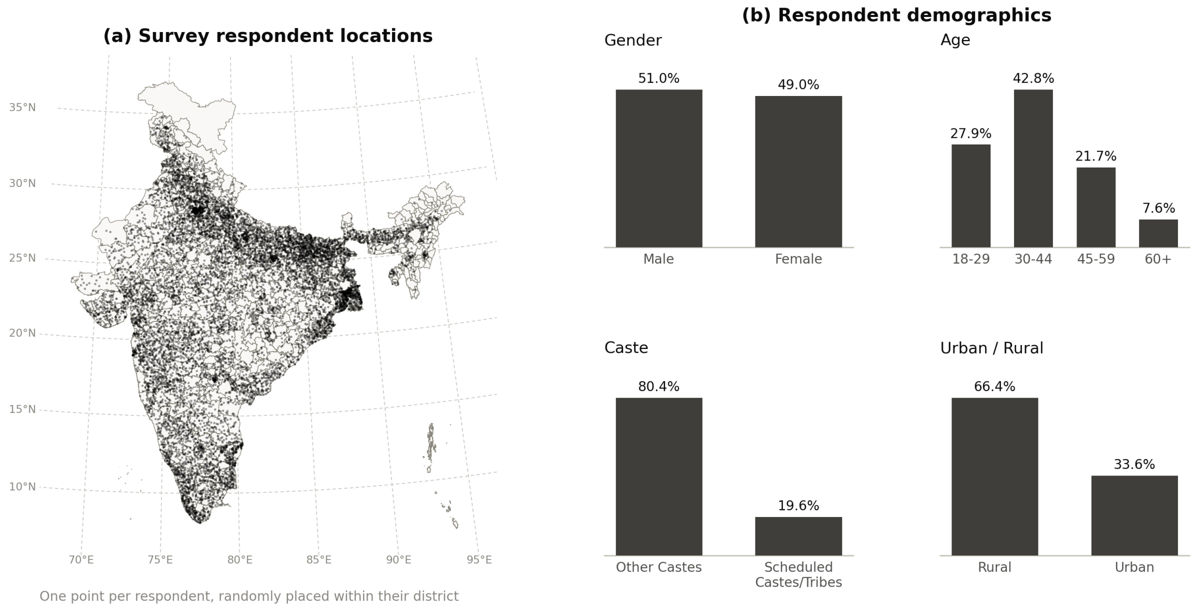

Figure A5: Survey coverage and respondent demographics. (a) Spatial distribution of survey respondents across India, with one point per respondent randomly placed within their district. (b) Respondent demographics: gender, age, caste, and urban/rural distributions.

Appendix A.2 News Media Coverage

We use the GDELT Global Knowledge Graph (GKG) (Leetaru & Schrodt, 2013) to construct a district-level panel of disaster-related news coverage in India from January 1 to November 30, 2024. GDELT monitors print, broadcast, and web news media in over 100 languages and processes article content in near real-time, extracting structured metadata including themes, locations, organizations, persons, and sentiment. Daily GKG files are downloaded and processed to yield article-level records.

To identify disaster-relevant coverage, we construct keyword dictionaries for flood- and drought-related events. Articles are classified accordingly if their GKG Themes field contains at least one corresponding keyword; those matching neither category are excluded, while those matching both are retained in each. Articles are then restricted to those referencing locations within India, with district and state identifiers extracted from the structured GKG Locations field. Only articles that can be unambiguously mapped to a valid Indian district and state using the boundary crosswalk described above are retained.

For each retained article, we extract six continuous sentiment indicators from the GKG Tone field and eight primary-emotion measures using the NRCLex library applied to the NRC Emotion Lexicon (Table A4). Emotion measures are computed as both shares (the fraction of total emotion word counts attributable to each emotion) and intensities (emotion word counts normalized by total article length). District-level measures are constructed by averaging article-level scores across all articles attributed to a given district within each time period.

Table A4: Media sentiment and emotion measures extracted per article.

Measure	**Definition**
Tone	Overall tone (positive minus negative sentiment)
Positive / Negative	Positive and negative sentiment scores
Polarity	Sum of positive and negative sentiment (emotional intensity)
Activity reference	Frequency of action-implying words
Self-group reference	Frequency of first-person plural references
Joy, fear, anger, sadness, disgust, surprise, trust, anticipation	NRC Emotion Lexicon categories, each computed as a share and an intensity

Appendix A.3 Physical and environmental covariates

Daily precipitation and temperature are derived from the ERA5 Reanalysis v5.0 (Hersbach et al., 2020), produced by the European Centre for Medium-Range Weather Forecasts (ECMWF). ERA5 provides hourly estimates of atmospheric variables at approximately 31 km horizontal resolution. For each district, we extract daily minimum, mean, and maximum values of total precipitation and 2 m air temperature for the full year 2024 and aggregate these to the district level by spatially averaging grid cells falling within each district boundary.

Nighttime light data were obtained from Visible Infrared Radiometer Suite (VIIRS) Day/Night Band (DNB) Monthly Composites Version 1 (VCMCFG). The data were produced by the Earth Observation Group at the Colorado School of Mines and distributed through the GEE data catalog (NOAA/VIIRS/DNB/MONTHLY_V1/VCMCFG) (Gorelick et al., 2017). The VCMCFG product provides cloud-free monthly composites of nighttime radiance at a native spatial resolution of approximately 463.8 m. The resulting map reveals the spatial distribution of artificial light across India, highlighting major metropolitan areas (Delhi, Mumbai, Bengaluru, Chennai, Kolkata, Hyderabad; Figure A6a).

District-level population density is derived from 2011 Census of India population counts divided by district area, providing spatial context for the urbanization and exposure patterns visible in the nighttime-light and flood-risk maps (Figure A6b).

Elevation data were obtained from the Shuttle Radar Topography Mission (SRTM) Version 3 Global 1 arc-second dataset (approximately 30 m resolution), accessed through the Google Earth Engine (GEE) data catalog (`USGS/SRTMGL1_003`) (Farr et al., 2007). River networks were derived from HydroSHEDS flow accumulation dataset at 15 arc-second resolution (approximately 500 m), accessed through GEE (`WWF/HydroSHEDS/15ACC`). HydroSHEDS (Hydrological data and maps based on SHuttle Elevation Derivatives at Multiple Scales) provides hydrologically conditioned elevation surfaces and derived products globally, generated from SRTM DEM (Lehner & Grill, 2013; Lehner et al., 2008). Flow accumulation values represent the number of upstream cells draining through each pixel, with higher values indicating larger rivers. To extract the visible river network, we applied a log transformation to the flow accumulation values and identified major rivers as pixels exceeding the 99.5th percentile of the log-transformed distribution (Figure A6c).

We incorporate analysis-ready geospatial embeddings from Google DeepMind's AlphaEarth model (Brown et al., 2025), which generates 64-dimensional continuous representations of land surface conditions from multi-spectral satellite imagery at 10m resolution for 2024. These embeddings encode a broad range of surface characteristics, including vegetation, soil, built environment, and water, without requiring explicit feature engineering. For each of the 64 embedding dimensions, we compute the minimum, mean, maximum, and key percentiles aggregated to the district level, yielding a rich set of data-driven environmental covariates.

District-level vulnerability to extreme weather is measured using the Climate Vulnerability Index developed by the Council on Energy, Environment, and Water (CEEW) (A. Mohanty & Wadhawan, 2021). The index is constructed as the product of exposure (the degree to which a district is subject to climate stressors based on historical climate and weather data) and sensitivity (the susceptibility of the population and systems to harm), divided by adaptive capacity (the ability to cope and recover). Higher values indicate greater net vulnerability. The index is standardized to a (-2,2) range by centering at the mean, scaling by the standard deviation, and capping values beyond two standard deviations to improve robustness to outliers.

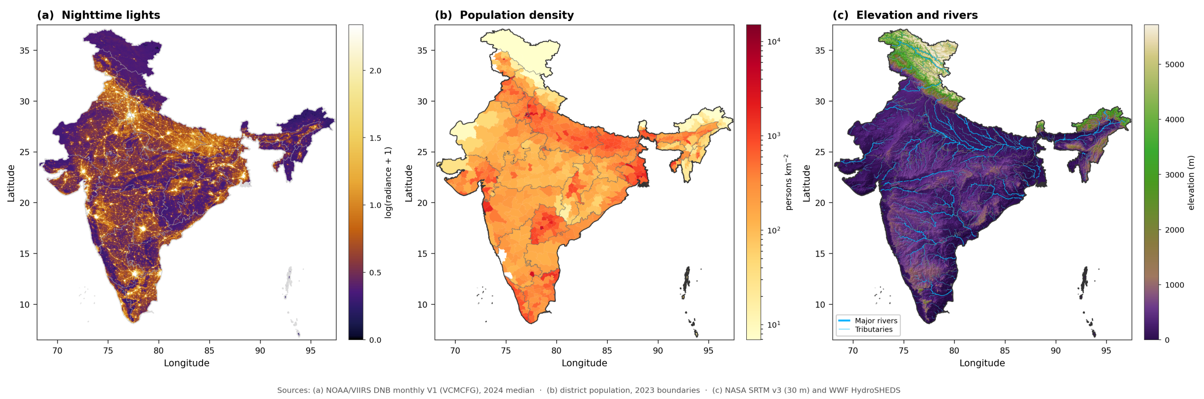

Figure A6: Physical and human-geography context layers across India. (a) Nighttime light radiance, 2024. (b) Population density, 2011 Census. (c) Elevation (SRTM DEM) with the extracted major river network (HydroSHEDS).

Appendix B Spatial Autocorrelation and Spatial Blocking

Perceived flood risk is likely to exhibit spatial dependence, as neighboring districts share similar environmental exposures, infrastructure conditions, media environments, and social networks that shape how communities experience and interpret flood hazards. We computed global Moran's I using row-standardized Queen contiguity spatial weights derived from the 2023 district boundary shapefile, with a k-nearest-neighbor ($k = 5$) fallback for island districts without contiguous neighbors. To complement this global measure, we applied Local Indicators of Spatial Autocorrelation (LISA), classifying each district as part of a High–High cluster, a Low–Low cluster, or a spatial outlier (High–Low or Low–High), based on 999 conditional permutations at a significance threshold of $p < 0.05$.

Perceived flood risk exhibits significant positive spatial autocorrelation across districts (global Moran's $I = 0.30$, $p < 0.001$, Queen contiguity). To characterize how this dependence varies with distance, we computed correlograms over exclusive 100 km distance rings with binary, row-standardized distance-band weights and 999 conditional permutations, for both perceived risk (raw district worry rates, which are independent of the model) and assessed risk. The two measures show distinct spatial regimes. Dependence in assessed risk is short-range: Moran's I falls from 0.33 among districts within 100 km to 0.17 at 100–200 km and 0.03 at 200–300 km, and is null or weakly negative at larger separations (Figure B7). Dependence in perceived risk decays more slowly (0.28 within 100 km, 0.22 at 100–200 km, 0.20 at 200–300 km) and remains detectable out to 800 km, consistent with the state-scale organization of risk perception documented in Appendix D rather than with purely local clustering.

Withholding entire spatial blocks, rather than randomly selected districts, ensures that no test district is adjacent to, or shares a block with, any training district. At this separation, spatial dependence in the physical hazard is effectively eliminated, and the dominant short-range component of dependence in perception is removed. The residual correlation between blocks reflects broad, state-scale structure that no feasible partition of a country spanning roughly 3,000 km could eliminate; because this residual structure makes held-out districts harder rather than easier to predict, spatial blocking yields a more conservative estimate of out-of-sample performance than random splitting.

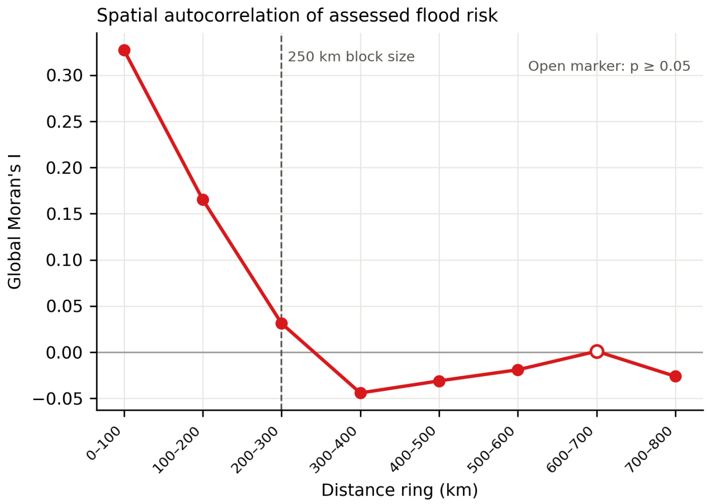

Figure B7: Moran's I values by distance for assessed risk.

Two sets of spatial features derived from this analysis enter the modeling framework as district-level covariates. First, spatial lag variables are computed as weighted averages of neighboring districts' values for flood worry and selected environmental indicators, capturing the influence of surrounding conditions on local perceptions. Second, LISA cluster classifications (High-High, Low-Low, High-Low, Low-High) are included as categorical covariates. Beyond their role as model inputs, these local, adjacency-based cluster designations are not used to characterize the alignment gap: the gap's systematic, non-random spatial structure is instead established directly by the state fixed-effects regression in Appendix D, which is scaled to administrative units rather than local adjacency.

Figure B8 reports the SHAP values summarizing each covariate's contribution to the final perceived-risk model, including the spatial lag and LISA features described above.

Appendix C Risk–Perception Alignment Typology

The main text classifies districts into four risk–perception alignment quadrants using the 633-district reporting universe (see Appendix A for how this population relates to the working shapefile). Each district is assigned based on whether its assessed risk (raw IMD flood count) and perceived risk fall above or below their respective district-level medians in this population (flood count = 23; perceived risk = 67.3%): Quadrant I (high assessed / low perceived), Quadrant II (high assessed / high perceived), Quadrant III (low assessed / high perceived), and Quadrant IV (low assessed / low perceived). This yields 160 (25.3%), 149 (23.5%), 168 (26.5%), and 156 (24.6%) districts respectively, summing to 633.

Per-state quadrant breakdown

Table C5 reports, for every state and union territory, the number and share of its districts falling in each quadrant, its overall mean alignment gap (assessed minus perceived, percentage points) and standard deviation, and its mean gap restricted to that state's Quadrant I districts specifically. States are sorted by overall mean gap, descending. Quadrant I's most-concentrated states in the main text are identified from the last column (mean gap among that state's own Quadrant I districts); Quadrants II–IV are instead described in the main text by within-state share, which can be read directly off this table's percentage columns for any state. All entries are computed on the same 633-district population and

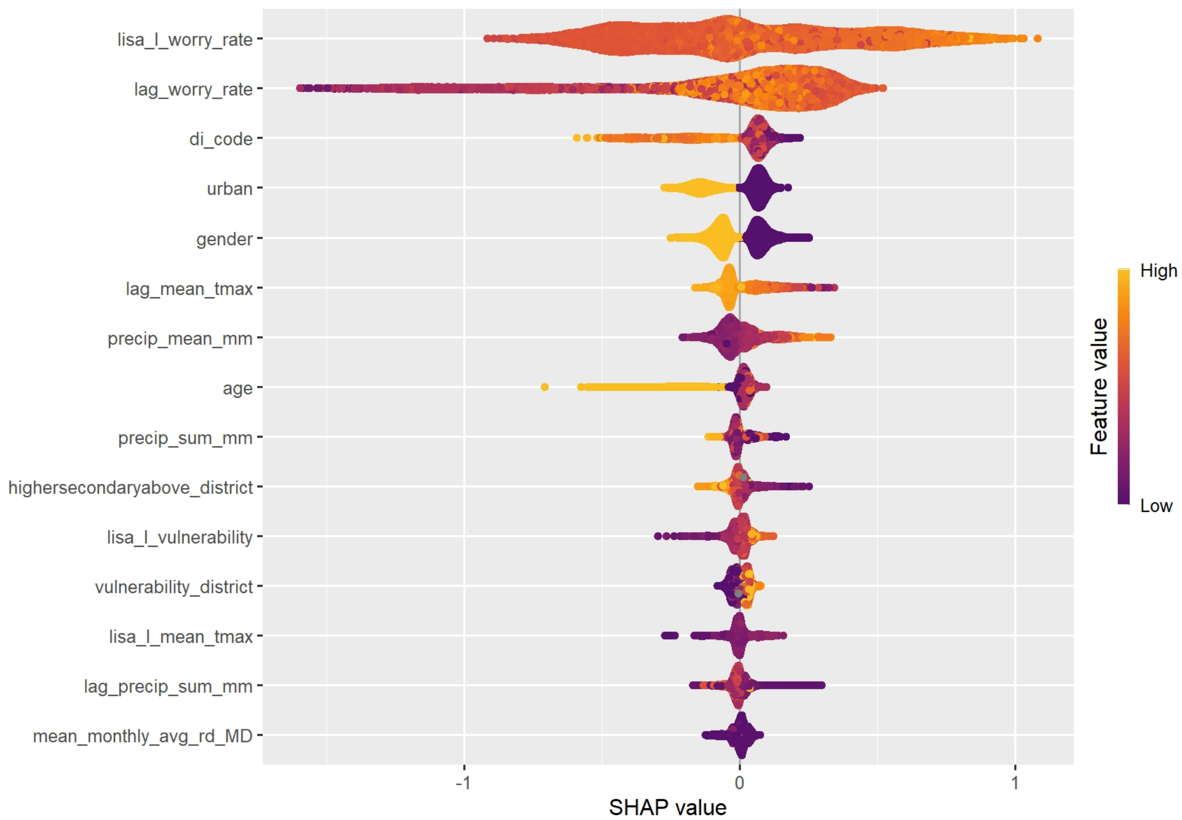

Figure B8: SHAP values of the covariates in the final perceived-risk model.

quadrant thresholds as the main-text typology, so the columns reconcile exactly with the quadrant totals reported there.

Appendix D Explaining the gap

To understand what explains the alignment gap, we modeled the signed gap (assessed minus perceived flood risk, in percentage points, where positive values denote under-perception) as a function of district-level environmental and socioeconomic covariates together with state fixed effects. The model specification is given in the Methods. Because a number of 2011 Census districts were later split into multiple present-day (2023-boundary) districts, we dissolved the 725 matched working-shapefile polygons to the 633 unique 2011 Census districts prior to fitting, averaging perceived risk, assessed risk, and all covariates across any split children of a given census district. The ten covariates were upstream flow accumulation, mean monthly monsoon rain-days, total monsoon precipitation, mean maximum temperature, the share of residents with higher-secondary education or above, the CEEW composite climate vulnerability index, news tone, flood-news article volume, the share of flood-related news coverage expressed with fear, and night-time light (mean radiance), each standardized to mean 0 and SD 1 prior to fitting. News tone, flood-news volume, and the fear share were missing for districts with insufficient news coverage to compute a score (52.8% of districts) and were median-imputed prior to standardization; night-time light coverage was complete. We estimated the model by ordinary least squares with HC1 heteroskedasticity-robust standard errors across all 633 districts with non-missing perceived and assessed risk.

Table D6 reports the full-model coefficients.

The alignment gap is organized at the state scale. Because that finding rests on a partition of districts into administrative units, it invites the question of whether states are doing substantive work or whether any partition of comparable resolution would absorb variation equally well. This section reports three checks. All are estimated on the same 633-district dissolved population and the same signed gap as the model above, with HC1 heteroskedasticity-robust standard errors throughout.

Table C5: Per-state breakdown of the risk–perception alignment typology ($N = 633$ districts; thresholds: flood count = 23, perceived risk = 67.3%). Q1–Q4: number of districts (share of that state's own districts) in each quadrant. Mean gap and SD gap are assessed minus perceived, in percentage points, positive values indicating under-perception, computed across all of a state's districts; SD is undefined for the single-district state (Chandigarh). Q1 mean gap is the same statistic restricted to a state's Quadrant I districts only, and is blank where a state has no Quadrant I districts. Sorted by overall mean gap, descending.

State/UT	N	Q1	Q2	Q3	Q4	Mean gap	SD gap	Q1 mean gap
Assam	27	14 (52%)	9 (33%)	1 (4%)	3 (11%)	+15.7	37.6	+35.3
Andhra Pradesh	13	9 (69%)	1 (8%)	0 (0%)	3 (23%)	+15.6	23.9	+29.0
Karnataka	30	20 (67%)	2 (7%)	0 (0%)	8 (27%)	+5.4	22.2	+15.2
Bihar	38	14 (37%)	24 (63%)	0 (0%)	0 (0%)	−4.9	16.5	+2.6
Kerala	14	5 (36%)	3 (21%)	2 (14%)	4 (29%)	−6.8	44.5	+33.5
Himachal Pradesh	12	2 (17%)	8 (67%)	2 (17%)	0 (0%)	−11.4	23.6	+2.5
Maharashtra	35	18 (51%)	9 (26%)	2 (6%)	6 (17%)	−13.5	23.3	+2.0
Telangana	10	3 (30%)	0 (0%)	0 (0%)	7 (70%)	−14.2	16.1	−4.5
Uttar Pradesh	71	27 (38%)	43 (61%)	1 (1%)	0 (0%)	−15.3	12.7	−9.9
Gujarat	26	5 (19%)	15 (58%)	4 (15%)	2 (8%)	−20.8	20.6	−5.1
Arunachal Pradesh	16	7 (44%)	0 (0%)	1 (6%)	8 (50%)	−21.4	16.6	−9.3
Tamil Nadu	32	6 (19%)	2 (6%)	7 (22%)	17 (53%)	−23.1	29.7	+22.6
West Bengal	19	7 (37%)	5 (26%)	3 (16%)	4 (21%)	−23.9	25.9	−11.9
Uttarakhand	13	4 (31%)	8 (62%)	1 (8%)	0 (0%)	−25.5	13.1	−16.7
Rajasthan	33	10 (30%)	7 (21%)	11 (33%)	5 (15%)	−28.8	19.3	−6.7
Goa	2	0 (0%)	1 (50%)	0 (0%)	1 (50%)	−33.4	2.6	—
Puducherry	4	0 (0%)	0 (0%)	0 (0%)	4 (100%)	−38.4	22.0	—
Odisha	30	4 (13%)	7 (23%)	10 (33%)	9 (30%)	−38.8	18.2	−11.1
Madhya Pradesh	50	3 (6%)	1 (2%)	28 (56%)	18 (36%)	−46.2	11.4	−22.8
Sikkim	4	0 (0%)	1 (25%)	1 (25%)	2 (50%)	−47.2	17.4	—
Punjab	20	0 (0%)	2 (10%)	14 (70%)	4 (20%)	−52.2	11.6	—
Jammu & Kashmir	20	1 (5%)	0 (0%)	16 (80%)	3 (15%)	−52.2	16.0	−5.3
Mizoram	8	0 (0%)	0 (0%)	1 (12%)	7 (88%)	−54.5	7.8	—
Haryana	21	0 (0%)	1 (5%)	18 (86%)	2 (10%)	−54.7	10.5	—
Nagaland	11	0 (0%)	0 (0%)	1 (9%)	10 (91%)	−56.6	5.5	—
Meghalaya	7	1 (14%)	0 (0%)	3 (43%)	3 (43%)	−58.4	21.1	−12.8
Manipur	9	0 (0%)	0 (0%)	2 (22%)	7 (78%)	−58.9	11.1	—
Chhattisgarh	18	0 (0%)	0 (0%)	13 (72%)	5 (28%)	−59.6	10.7	—
Delhi	9	0 (0%)	0 (0%)	9 (100%)	0 (0%)	−60.5	3.5	—
Jharkhand	24	0 (0%)	0 (0%)	11 (46%)	13 (54%)	−62.8	6.4	—
Chandigarh	1	0 (0%)	0 (0%)	0 (0%)	1 (100%)	−64.7	—	—
Dadra & Nagar Haveli & Daman & Diu	2	0 (0%)	0 (0%)	2 (100%)	0 (0%)	−70.5	1.1	—
Tripura	4	0 (0%)	0 (0%)	4 (100%)	0 (0%)	−74.6	4.5	—

Appendix D.1 Comparison with a physical-geography partition

If state fixed effects were standing in for physical geography, a partition drawn along hydrological rather than administrative lines should perform comparably. We tested this using the Central Water Commission's river basin boundaries (National Water Informatics Centre, 2025), which delineate 25 basins nationally. Districts were assigned to basins by largest area of intersection in an equal-area projection (EPSG:7755, the basin file's native CRS). All 633 districts received an assignment, with a mean overlap share of 92.8% and a median of 100%; 39 districts (6.2%) fell below 60% overlap and are flagged as ambiguous. Reassigning districts by geometric centroid rather than majority area changed the assignment of 15 districts (2.4%), leaving the results below unchanged. Twenty-two basins received at least one district, and no basin contained only one.

Basins explain substantially less of the gap than states do (Table D7). Basin fixed effects alone account for 23.1% of the variance in the gap, against 57.9% for state fixed effects, despite a comparable number of groups. Adding basin fixed effects on top of state fixed effects raises adjusted R^2 by 0.001, and the basin dummies are jointly insignificant once state is controlled for ($F = 1.17$, $p = 0.270$). The state partition therefore subsumes the basin partition rather than competing with it.

Table D6: Full-model coefficients for the alignment gap (OLS, HC1 robust standard errors). Positive values indicate greater under-perception. $^*p < 0.05$.

Term	β	SE	p	95% CI
Night-time light (mean radiance)	-5.19^*	1.90	0.006	$[-8.91, -1.47]$
Flood-news article count	$+3.54^*$	1.51	0.019	$[0.57, 6.50]$
News tone (valence)	-0.91	0.91	0.316	$[-2.69, 0.87]$
News emotion: fear (share)	-0.85	0.91	0.350	$[-2.65, 0.94]$
CEEW vulnerability index	$+0.67$	0.98	0.495	$[-1.25, 2.58]$
Mean maximum temperature	-0.67	1.49	0.652	$[-3.60, 2.25]$
Higher-secondary educated (%)	-0.12	1.02	0.907	$[-2.12, 1.88]$
Monsoon precipitation	-0.15	1.32	0.908	$[-2.74, 2.43]$
Monsoon rain-days	-0.15	1.39	0.913	$[-2.87, 2.57]$
Flow accumulation	-0.05	0.81	0.949	$[-1.64, 1.53]$
Intercept	$+14.39$	6.98	0.039	$[0.71, 28.08]$
State fixed effects (32 dummies, 33 states)		jointly $p < 0.001$		

One feature of the basin partition bears noting. The Ganga basin contains 223 of the 633 districts, so a large share of the country falls into a single undifferentiated group. This limits how much variance the basin partition can absorb by construction. The conditional test in the final row of Table D7, which holds state fixed and asks what basins add, is not subject to this limitation.

Table D7: River basins compared with states as partitions of the alignment gap ($N = 633$ districts). Basin assignments follow the Central Water Commission boundaries.

Specification	R^2	adj. R^2	AIC	BIC	Groups
Covariates only	0.200	0.187	5971.7	6020.7	—
Basin FE only	0.231	0.204	5968.9	6066.8	22
Covariates + basin FE	0.333	0.298	5899.0	6041.4	22
State FE only	0.579	0.556	5609.8	5756.7	33
State + basin FE	0.595	0.557	5627.5	5867.8	54

Appendix D.2 Comparison with random partitions of equal resolution

Any partition into 33 groups absorbs some variance simply by introducing 32 parameters. To establish that the state result is not an artifact of resolution, we generated 1,000 random partitions of the 633 districts into 33 groups, drawn to match the size distribution of the actual states (1 to 71 districts per group), and fit the fixed-effects-only specification to each. We ran two variants. In the first, districts were assigned to groups at random without regard to geography. In the second, groups were grown outward from random seeds along Queen contiguity edges, so that the resulting groups are spatially coherent and therefore a more demanding comparison.

The observed state fixed effects explain more of the gap than every one of the 2,000 random partitions (Table D8). Under the naive variant, the null distribution of R^2 has a mean of 0.051 and a maximum of 0.099 against an observed value of 0.579. Under the spatially contiguous variant, the null mean is 0.196 and the maximum 0.289, still well below the observed value, and the observed adjusted R^2 of 0.556 is more than double the null maximum of 0.251. In both variants no draw reached the observed value (0 of 1,000). Figure D9 shows the two null distributions against the observed value.

In the contiguous variant, groups occasionally become enclosed by their neighbours before reaching their target size, and the remaining districts are then placed at random. This affected a mean of 127 districts (20%) per draw. The effect is to make the null partitions less spatially coherent than intended, which lowers rather than raises the null distribution, so the comparison above is conservative with respect to the state result.

Appendix D.3 Residual spatial autocorrelation

If state fixed effects were an arbitrary partition, spatial structure in the gap would survive their inclusion. We computed global Moran's I on the residuals of each specification, using the same row-standardized Queen contiguity weights and 999 conditional permutations as Appendix B.

Table D8: Observed state fixed effects against null distributions from 1,000 random partitions per variant (2,000 in total) of the 633 districts into 33 groups matching the state size distribution.

Variant	Null mean R^2	Null max R^2	Null mean adj. R^2	Null max adj. R^2	Draws $\geq$ observed
Naive random	0.051	0.099	0.000	0.051	0 of 1,000
Spatially contiguous	0.196	0.289	0.154	0.251	0 of 1,000
Observed state $R^2 = 0.579$; adjusted $R^2 = 0.556$.					

Residuals from the covariates-only model retain strong positive spatial autocorrelation ($I = 0.262$, $p < 0.001$), confirming that the ten district-level covariates leave the gap's spatial structure unexplained. Once state fixed effects are included, that structure is no longer detectable ($I = -0.020$, $p = 0.731$ for state fixed effects alone; $I = -0.018$, $p = 0.737$ for the full model). A correlogram over 100 km distance rings shows that full-model residuals remain flat and insignificant at every separation out to 800 km ($|I| \leq 0.039$, all $p > 0.2$). State fixed effects therefore absorb the spatial dependence in the gap rather than partitioning it arbitrarily.

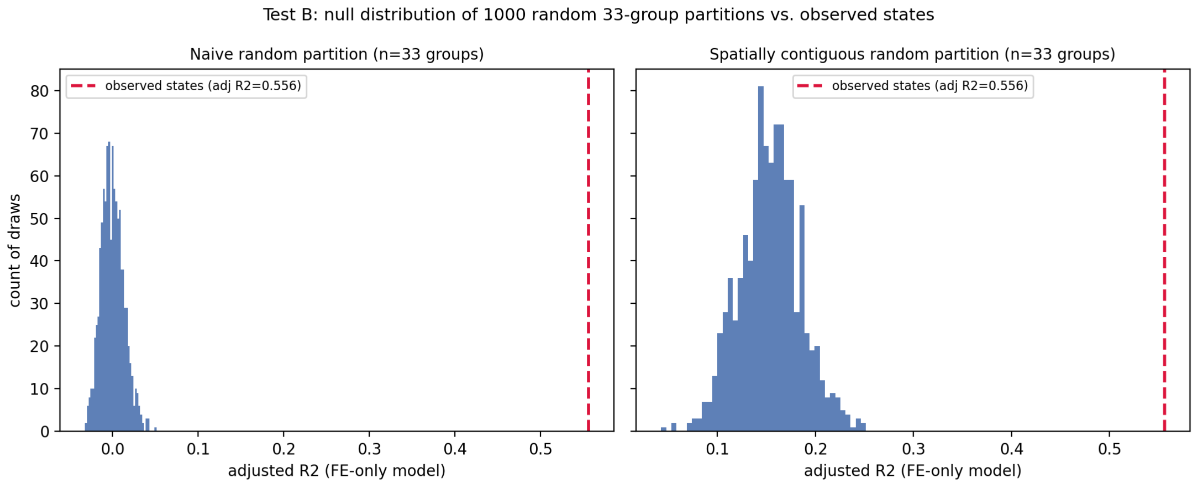

Figure D9: Null distribution of adjusted R^2 (fixed-effects-only specification) from 1,000 random partitions per variant (2,000 in total) of the 633 districts into 33 groups matching the state size distribution, under the naive (left) and spatially contiguous (right) variants. The dashed line in each panel marks the observed state fixed-effects value (adjusted $R^2 = 0.556$); no draw in either variant reaches it.

Appendix E Sensitivity to the normalization of assessed risk

The level of the gap depends on how the flood count is normalized, as noted in the main text. The variance decomposition is not strictly invariant to that choice either, because rescaling assessed risk changes how much of the gap's variance originates in the assessed rather than the perceived component. We therefore recomputed the gap under five normalizations of the flood count and re-estimated the state fixed-effects specification for each.

The state fixed-effects share of variance ranges from 55.5% to 60.0% across all five (Table E9). The conclusion that the gap is organized at the state scale does not depend on the normalization used.

Table E9: State fixed-effects variance share under alternative normalizations of the flood count.

Normalization	R^2	adj. R^2
Clipped at 95th percentile*	0.582	0.560
Min–max over full range	0.565	0.542
Percentile rank	0.600	0.578
z-score, rescaled	0.555	0.532
$\log(1 + \text{count})$, min–max	0.587	0.565

* All rows recompute assessed risk after dissolving, so this row differs slightly from Table 2, which normalizes before dissolving.